31st Annual International Conference of the IEEE EMBS
Minneapolis, Minnesota, USA, September 2-6, 2009

A method for morphological characterization of dural ectasia in Marfan syndrome

Maria I. Iacono, Katia Passera, Lorenzo Magrassi, Roberto Dore,
Paolo Lago, Eloisa Arbustini and Luca T. Mainardi

Abstract— **In this paper we reported a novel method to detect and quantify dural ectasia in Marfan syndrome. Firstly, the dural sacs of 8 Marfan patients were segmented by applying an unsupervised Fuzzy C-Means method on T2-weighed magnetic resonance images. Then, for each patient a tubular model of the dural sac was extracted by detecting and removing the existent pathological extrusions. The segmented images together with the resulting tube were then rendered using a marching cubes algorithm. The proposed algorithm represents a first attempt to quantify and to morphologically characterize the pathological ectasia that usually accompanies the Marfan disorder. The generated 3D reconstruction and the opportunity to overlap them with a physiological model provides the clinician with a tool for a panoramic view of the structures and a means for a more accurate inspection of ectasia. In addition the extracted parameters furnish quantitative and reproducible measures that could be useful as discriminative indexes for an automatic and more objective diagnosis.**

I. Introduction

ACCORDING to the Ghent nosology [1], dural ectasia is considered one of the major criteria in the diagnosis of Marfan syndrome. Dural ectasia is defined as a widening of the dural sac, which is a membrane enwrapping the spinal cord, with consequent expansion of the spinal canal.

Diagnosis of dural ectasia is based on the visual assessment of magnetic resonance (MR) or computed tomography (CT) images. Clinical importance of a more accurate ectasia analysis lies in the fact that the cases of mild ectasia represent often a diagnostic dilemma and they cannot easily evaluated by the only visual inspection. Then, the quantification of the degree of the ectasia could be useful as discriminative index for an automatic identification of pathological cases.

A first attempt to provide more objective and reproducible methods for the quantitative assessment of the dural ectasia was given by Villeirs et al. [2]. A cut-off value of the ratio of transverse latero-lateral diameter of the dural sac and vertebral body, manually outlined on sequential CT slices by the radiologist, was given as threshold for assuming an abnormal dural sac volume. Oosterhof et al. [3], proposed to compute dural sac ratios in the antero-posterior plane, at the levels of L3 and S1, while Söylen et al. [4] proposed the bidimensional product of the transverse and sagittal widths of the dura at three levels of each vertebral body from L1 to S1.

However, the proposed measures are considerably variable because of their not automatic nature and moreover they do not take into account the three-dimensionality.

Ahn et al. [5], [6] were the first to suggest the computation of the volume as the "gold standard" for the diagnosis using MR data; however, because techniques to calculate dural volume from MR images were not widely available, they identify two major criteria and two minor criteria based on monodimensional measures and on visual assessment of particular features.

The main difficulty in obtaining dural volume stems from the fact that often images are corrupted by artifacts such as the partial volume effect and bias field distortion. In these conditions, classical segmentation algorithms [7], like thresholding, region growing and contour extraction may produce unreliable results.

Therefore, more advanced techniques affording the automatic segmentation of inhomogeneous structure, like clustering algorithms, should be applied.

This paper reports preliminary analyses aimed at developing a system to morphologically characterize pathological dural sacs and to provide for easier detection of dural ectasia.

The method is based on the recognition and the extraction of the dural sac by a Fuzzy C-Means (FCM) segmentation and on its quantitative comparison with a regular tubular structure modeling the dura. A simultaneous 3D visualization of the segmented dural sac and of the physiological model enables to localize the areas where the two structures overlap and to qualitatively assess the presence of pathological extrusions.

Manuscript received April 23, 2009.

M. I. Iacono is with the Biomedical Engineering Department, Politecnico di Milano, Italy (phone: +39-02-2399-9507; fax: +39-02-2399-3360; e-mail: maria.iacono@mail.polimi.it).

K. Passera is with the Biomedical Engineering Department, Politecnico di Milano, Italy.

L. Magrassi is with the Neurosurgery Dep. Surgical Science Università di Pavia, Fondazione IRCCS Policlinico S. Matteo, Pavia, Italy.

R. Dore is with the Department of Radiology and the Interdisciplinary Group for Marfan Syndrome (GISM), Fondazione IRCCS Policlinico S. Matteo, Pavia, Italy.

P. Lago is with the Engineering Department, Fondazione IRCCS Policlinico S. Matteo, Pavia, Italy.

E. Arbustini is with the Cardiovascular Pathology and Molecular Diagnostic Lab and the Interdisciplinary Group for Marfan Syndrome (GISM), Fondazione IRCCS Policlinico San Matteo, Pavia, Italy.

L. T. Mainardi is with the Biomedical Engineering Department, Politecnico di Milano, Italy.

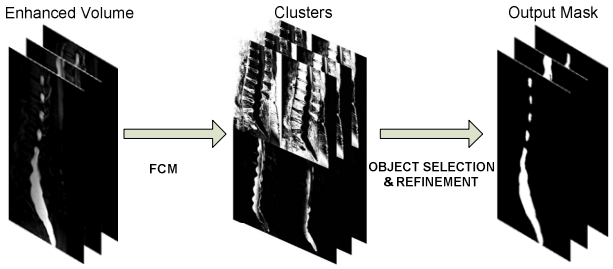

Fig. 1. Scheme of the segmentation method

II. Materials and Methods

A. Experimental protocol

MR images of the patients were acquired in the Department of Radiology of the Fondazione IRCCS Policlinico S. Matteo in Pavia. In all patients the clinical diagnosis of Marfan syndrome was confirmed by mutation analysis of the fibrillin gene.

The segmentation algorithm, the morphological analysis, and the subsequent volumetric reconstruction were applied on 8 patients affected by Marfan syndrome.

Each patient underwent MR scanning of the lumbo-sacral spine using a 1.5 T Siemens closed scanner. The following sequence was performed: sagittal T2-weighed fat saturated spin echo with a spatial resolution of 0.781 mm x 0.781 mm in the sagittal plane, a slice thickness of 4 mm, and an inter-slice gap of 4.4 mm.

B. Dura extraction

Images were pre-processed in order to enhance their contrast detail for the segmentation process. Firstly, a Non-parametric Non-uniform intensity Normalization (N3) algorithm aimed at removing radio-frequency inhomogeneities, shading artifacts, or intensity non-uniformities was applied to the images [8]. In addition, a contrast enhancement step (grey levels stretching) and a median filtering were performed.

The pre-processed volume is segmented by applying an unsupervised FCM algorithm [9], [10].

The algorithm aims to find the partition of a data set $\mathbf{X}=\{x_1, x_2, ...x_n\}$ into c clusters.

The partition is represented by a $(c \times n)$ partition matrix U. The element, $u_{ik}(1 \le i \le c, 1 \le k \le n)$ of the matrix represents the membership of the k^{th} data point in the i^{th} class in a continuous range from 0 to 1. This fuzzy membership characterizes the degree of similarity between the k^{th} point and the i^{th} cluster.

The partition matrix is computed by minimizing the intra-groups square error function J_m:

$$J_m = \sum_{i=1}^{c}\sum_{k=1}^{n} u_{ik}^{m} \left\| \mathbf{X}_k - \mathbf{V}_i \right\|^2 \qquad (1)$$

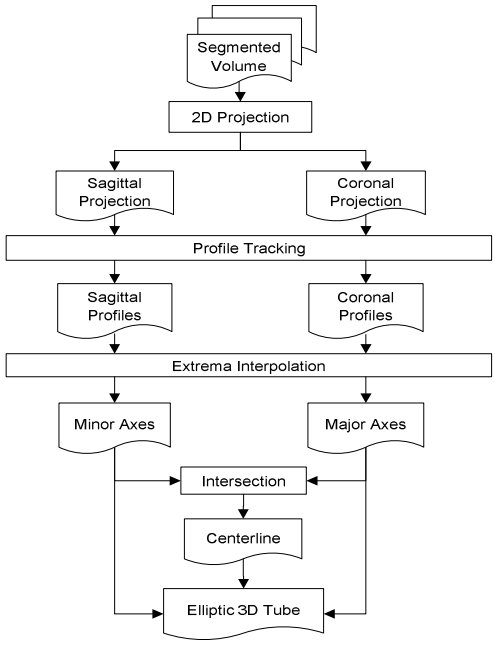

Fig. 2. Tube modeling workflow

Where $\mathbf{V}_i = \{V_1, V_2, ...V_c\}$ are the randomly initialized cluster centers and $m \in [1, \infty)$ is the fuzzyfication index. In this work it was set to 2.

In Fig. 1 the result of our segmentation approach is shown. The enhanced volume is segmented by applying the FCM algorithm. For this application, a different number of clusters were evaluated. The optimal structure differentiation was obtained using 6 clusters.

After having applied FCM on the volume, each pixel is assigned to a specific cluster for which the degree of membership is maximal.

This allows for the labeling of every pixel and the identification of the regions belonging to the dura. An accurate segmentation of the dural sac can be obtained by extracting the pixels belonging to the three clusters characterized by the highest centroids values and corresponding to the brightest gray levels. Pixels belonging to a fourth cluster and representing the darkest areas of the region of interest, namely the nerve roots that run within the dural sac, were included into the selected area if spatially connected with it.

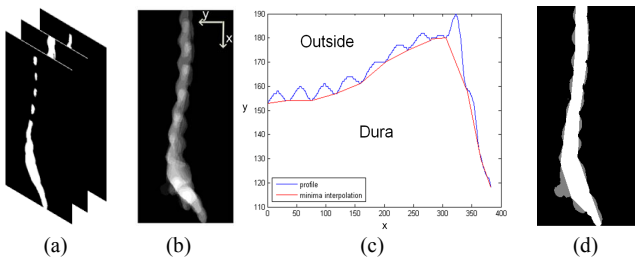

Fig. 3. (a) The segmented dura, (b) the sagittal projection of the volume with the coordinate system, (c) the left profile of the dura projection and (d) the output mask (in white).

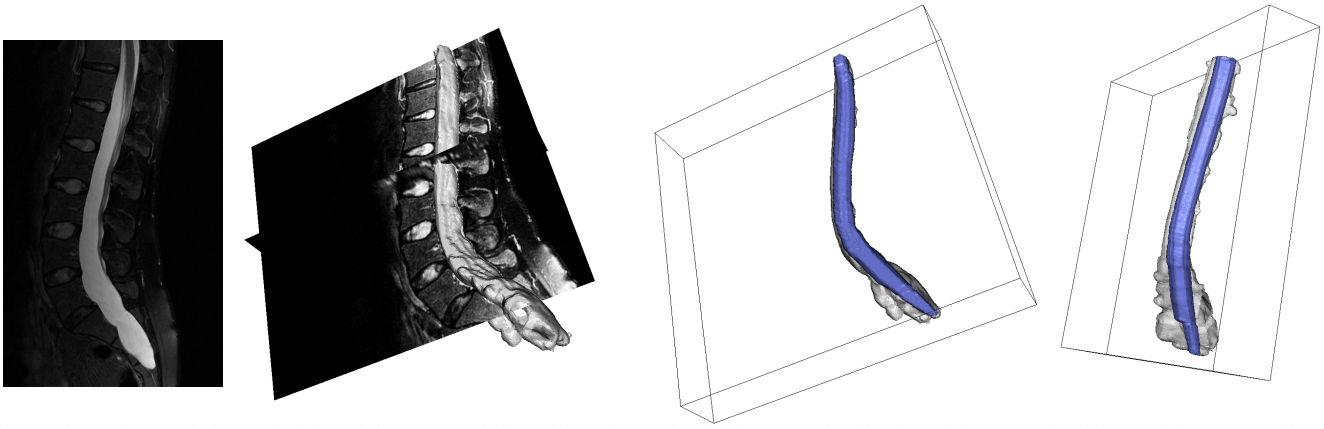

Fig. 4. The surface rendering tool. (left to right) A sagittal slice of the volume, the simultaneous visualization of the 3D rendered dura and the 2D RM slices, the overlap of the rendered dura and the physiological model in two different views.

Finally, the segmented dura was refined using morphological operations in order to obtain a more accurate result.

C. Tubular structure modeling

In order to reproduce an approximated model of the hypothetical silhouette of the dura in absence of pathology, an elliptical tube, fitting the dural sac, was formulated. Fig. 2 shows the tube modeling workflow.

To compute the major and minor axes of the elliptical and variable cross-sections of the tube, the volume was projected on the sagittal and coronal planes, resulting in two bidimensional images representing the maximum extents of the dura in those projections.

For each projection the left and the right profiles of the dura were obtained by tracking its edges in the y direction.

In order to separate the pathological extrusions from the dura body, the local extrema of each profile were spline-interpolated to estimate the values of the profile on the removed points. In Fig. 3 the projection (b), the extrema interpolation of the left profile of the dura (c) and the resulting mask (d) related to the sagittal plane are shown as example of the process.

The elliptical cross-sections of the tube were constructed using as minor and major axes the diameters obtained as distances between the interpolated profiles in the sagittal and in the coronal views, respectively.

Therefore, the sagittal and the coronal diameters were intersected in order to obtain the centerline of the tube.

D. Surface rendering

To construct an optical volumetric rendering of the segmented data and of the tubular structure, the open-source Visualization ToolKit (VTK) [11], was used.

Each volume, which is available as a set of monochrome images, is filtered using a Marching Cubes algorithm [12] with the aim of generating isosurfaces from the data.

In order to reduce the number of polygons to be rendered, the resultant polygonal surface is simplified with a decimation algorithm, with the constraint of the preservation of the topology of the structure.

The decimated polygonal surface is smoothed by adjusting the coordinates of the vertices using Laplacian smoothing. This step has the effect of relaxing the mesh, making the cells better shaped and the vertices more evenly distributed.

III. Results

Fig. 4 shows in a rendering window the resulting 3D reconstruction of the segmented dural sac and of the physiological dura model of a patient affected by Marfan syndrome. The implemented tool furnishes a simultaneous 2D/3D visualization by locating the 3D reconstructed volumes inside the real MR slices. This enables not only the visual comparison of the dura with the reference model but also its interrelation with the surrounding structures and a consequent better understanding of mutual interactions involved.

By navigating the volumes it is possible to have a compact representation of dura geometry and a resulting visual tool for the assessment and the localization of shape anomalies, such as protrusions.

In addition, the method permits one to quantify the dural ectasia volume and then provides an index to assess the severity degree of the pathology.

TABLE I
ECTASIA QUANTIFICATION

PATIENTS	EC_{cran} *(%)*	EC_{med} *(%)*	EC_{caud} *(%)*
1	47.11	32.20	20.69
2	17.82	24.25	57.93
3	23.69	21.19	55.12
4	36.40	16.82	46.78
5	25.39	36.19	38.42
6	30.57	33.34	36.09
7	15.48	11.58	72.94
8	25.12	33.74	41.14

Table I summarizes results obtained for the 8 analyzed patients. The ectasia volume is calculated as the difference between the real volume obtained via the segmentation and the tube volume considered as the physiological reference volume. Furthermore, the volume containing the dura was divided into three blocks equal in length in a cranial-caudal direction and the percentage contributions to the global ectasia of those three different portions of the dura – the cranial, the medial and the caudal portions-, EC_{cran}, EC_{med}, and EC_{caud}, respectively, were extracted in order to evaluate the spatial distribution of the extrusions.

In almost all the cases the degree of ectasia is the highest in the caudal portion, as expected.

IV. Conclusions

We have proposed a method for the automatic extraction, morphological characterization, and visualization of the dural sac of Marfan patients based on a 3D segmentation procedure followed by a dura modeling and a surface rendering algorithm.

This work represents a preliminary method for the morphological characterization of pathological dural sacs with the objective of providing the clinician with quantitative parameters that synthetically describe surface irregularity, classify the degree of severity, and ensure a more objective and accurate diagnosis.

The implemented tool enables the clinician to automatically obtain a quantitative measure of the dura ectasia. In addition, it is a visual instrument which permits a general and concise view of the structures, their localization in space and their comparison with an elliptic tubular structure that models the dura.

In addition the accurate localization of pathological excrescences can be of aid for a better comprehension of symptoms like back pain or abdominal pain, which are often related to this disorder and whose causes are still the object of study and research.

The limited number of patients and the sub-optimal spatial resolution of the images do not enable a quantitative validation and assessment of the accuracy of the method. However, this paper represents a first attempt to approach the problem and further investigations will be done, including a comparative analysis with the existing methods proposed by literature and based on the manual outlining of the diameters [2], [3], [4], [5], [6].

Nevertheless our initial results are encouraging, consistent with the clinical evaluation, and result useful for a more accurate assessment of the severity of dura widening.

References

[1] A. De Paepe, R. B. Devereux, H. C. Dietz, R. C. M. Hennekam, R. E. Pyeritz, "Revised diagnostic criteria for the Marfan syndrome,". *Am J Med Genet*, vol. 62, pp. 417–426, 1996.

[2] G. M. Villeirs, A. J. Van Tongerloo, K. L. Verstraete, et al., "Widening of the spinal canal and dural ectasia in Marfan's syndrome: assessment by CT," *Neuroradiology*, vol. 41, pp. 850-854, 1999.

[3] T. Oosterhof, M. Groenink, F. J. Hulsmans, et al., "Quantitative assessment of dural ectasia as a marker for Marfan syndrome," *Radiology*, vol. 220, pp. 514-518, 2001.

[4] B. Söylen, K. Hinz, J. Prokein, et al., "Performance of a new quantitative method for assessing dural ectasia in patients with FBN1 mutations and clinical features of Marfan syndrome", *Neuroradiology*, vol. 51, pp. 397–400, 2009.

[5] N. U. Ahn, P. D. Sponseller, U. M. Ahn, et al., "Dural ectasia in the Marfan syndrome: MRI and CT findings and criteria," *Genet Med*, vol. 2, pp. 173-179, 2000.

[6] N. U. Ahn, P. D. Sponseller, U. M. Ahn, et al., "Dural ectasia is associated with back pain in Marfan syndrome," *Spine*, vol. 25, pp. 1562-1568, 2000

[7] L. P. Clarcke, R. P. Velthuizen, M. A. Camacho, et al., "MRI segmentation: methods and applications," *Magn. Reson. Imag.*, vol. 13, pp. 343-368, 1995.

[8] J. G. Sled, A. P. Zijdenbos, A. C. Evans, "A non-parametric method for automatic correction of intensity non-uniformity in MRI data," *IEEE Trans. on Medical Imaging*, vol. 17, pp. 87-97, 1998.

[9] J. C. Bezdek, "Pattern Recognition with Fuzzy Objective Function Algorithms," Plenum Press, NY, 1981.

[10] J. C. Bezdek, S. K. Pal, "Fuzzy Models for Pattern Recognition", IEEE Press, NY, 1992.

[11] The Visualization Toolkit at http://www.kitware.com

[12] W. E. Lorensen,H. E. Cline, "Marching cubes: A high resolution 3D surface construction algorithm," *Computer Graphics*, vol. 21(4), pp. 163-169, 1987.